PNAS
www.pnas.org

Supplementary Information for

Neoproterozoic to early Phanerozoic rise in island arc redox state due to deep ocean oxygenation and increased marine sulfate levels

Daniel A. Stolper and Claire E. Bucholz

Corresponding Authors: Daniel A. Stolper and Claire E. Bucholz
Email: dstolper@berkeley.edu and cbucholz@caltech.edu

This PDF file includes:

Supplementary Information Text
Figs. S1 to S11
Tables S1 to S2
References for SI reference citations

Other supplementary materials for this manuscript include the following:

Datasets S1 to S5

www.pnas.org/cgi/doi/10.1073/pnas.1821847116

Supplementary Information Text

Description of mantle melting model to determine how V/Sc and $Fe^{3+}/\Sigma Fe$ ratios vary as a function of fO_2, degree of melting, modal mineralogy, and initial source V/Sc ratio.

Here we describe the model used to generate points in Figures S9 and S10. The model calculates V/Sc and $Fe^{3+}/\Sigma Fe$ ratios of melts as a function of degree melting, modal mineralogy of the source rock, initial V/Sc ratio of the source rock, and the fO_2 of the source rock. We assume melt generation in the pressures of the spinel stability field, which is thought to be generally applicable for basalts generated in subduction zones based on their trace element signatures which do not indicate residual garnet (e.g., ref. 1). In addition, the dependency of V partitioning between garnet and melt as a function of fO_2 and garnet composition is not well known, rendering quantitative modeling of garnet lherzolite melting difficult.

V/Sc ratios were calculated using the non-modal melting equations of (2) and the spinel-lherzolite melting reaction coefficients of (3) from their 1.5 GPa experiments L134-L138 ($0.13opx + 0.89cpx + 0.12sp$ = liquid + $0.13ol$; see Table 4 in ref. 3). This choice of conditions is relevant for spinel lherzolite melting up to 24% melt and consistent with previous choices for V/Sc modeling during partial melting of spinel lherzolites (4). Two spinel lherzolites compositions characterized by different initial modal mineral abundances were modeled: (*i*) a depleted "MORB-like" mantle source with 60% olivine, 20% orthopyroxene, 15% clinopyroxene, and 5% spinel (green diamonds/curves in Figures S9 and S10) and (*ii*) a further depleted "arc-like" mantle source calculated after 10% depletion of the "MORB-like" mantle source with 66.3% olivine, 20.6% orthopyroxene, 8.7% clinopyroxene, and 4.4% spinel (red and blue dots/curves in Figures S9 and S10).

For mantle source (*i*) we assumed initial V and Sc concentrations of 79 and 16.3 ppm, respectively, after MORB mantle values of (5), giving a V/Sc ratio of ~4.9. For mantle source (*ii*) we used two initial sets of V and Sc concentrations: (a) V = 79, Sc = 16.3 (red dots/curves, V/Sc = 4.9; as for mantle source *i*) and (b) V = 50, Sc = 13.5 (blue dots/curves, V/Sc = 3.7). The second choice of V and Sc ratios was chosen following (4) and is meant to represent a more depleted source region, consistent with the more depleted modal mineralogy. Forward modeling of melt V and Sc concentrations was calculated at 1% melting intervals. V and Sc mineral-melt partition coefficients are from (6) at oxygen fugacity values relative to the quartz-fayalite-magnetite (QFM) buffer of QFM-1 to +4. Results at 10 (open symbols) and 20% (filled symbols) partial melting (F) are shown.

$Fe^{3+}/\Sigma Fe$ ratios were calculated independently from V/Sc ratios. The average primary melt composition for Pagan volcano, Mariana arc (see Appendix F of ref. 7) was used as a representative primary arc basalt. The equilibrium $Fe^{3+}/\Sigma Fe$ ratio of this composition at various oxygen fugacities was calculated according to (8) at 1100ºC and 1000 bars. The QFM buffer was calculated using the formulation of (9).

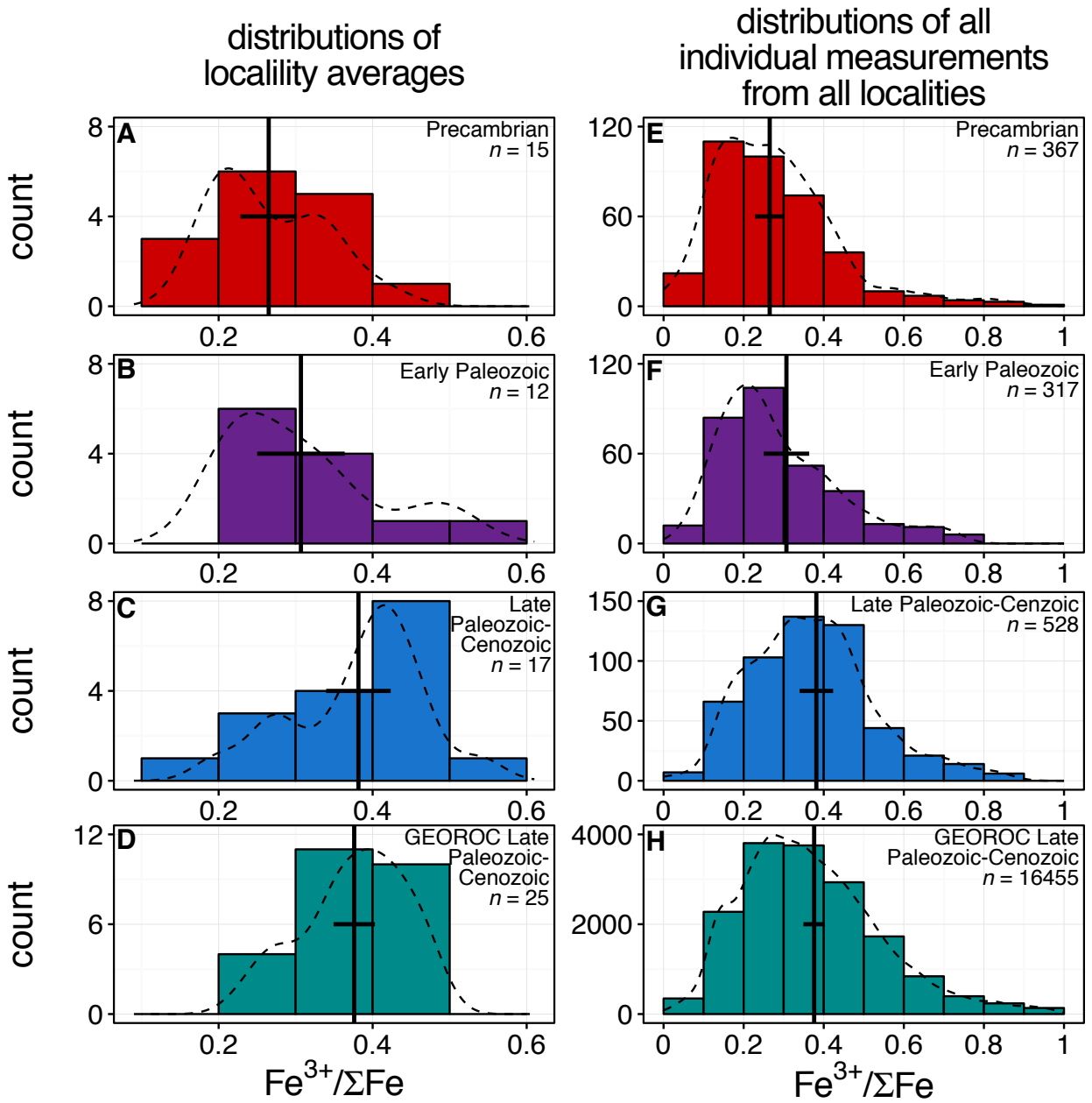

Fig. S1: Histograms of $Fe^{3+}/\Sigma Fe$ data. A-D are histograms of the locality averages (as given in Fig. 1). E-H are histograms of every individual data point used to calculate the locality averages. Black vertical lines are the average value of the locality averages for a given age range with 2 SE error bars as given in Fig. 1. *n* is the number of data points. Dotted lines are smoothed distributions. A shift in the mean and mode of the distributions to higher $Fe^{3+}/\Sigma Fe$ values for the Late Paleozoic-Cenozoic samples both from our compilation and the GEOROC database relative to earlier time frames (Early Paleozoic and Precambrian) is clearly apparent for the locality averages. This is also apparent in the histograms of individual data points (E-H), but is less visually obvious. This is in part due to the presence of the tail in the distributions to elevated $Fe^{3+}/\Sigma Fe$ values (>0.6), which, as discussed in the main text, we interpret to be due to the oxidation of a small number of samples at the Earth's surface in the recent past (i.e., during exposure on land before sample collection). As also discussed in the main text, the presence of this tail has no effect on our interpretations (see Table S1).

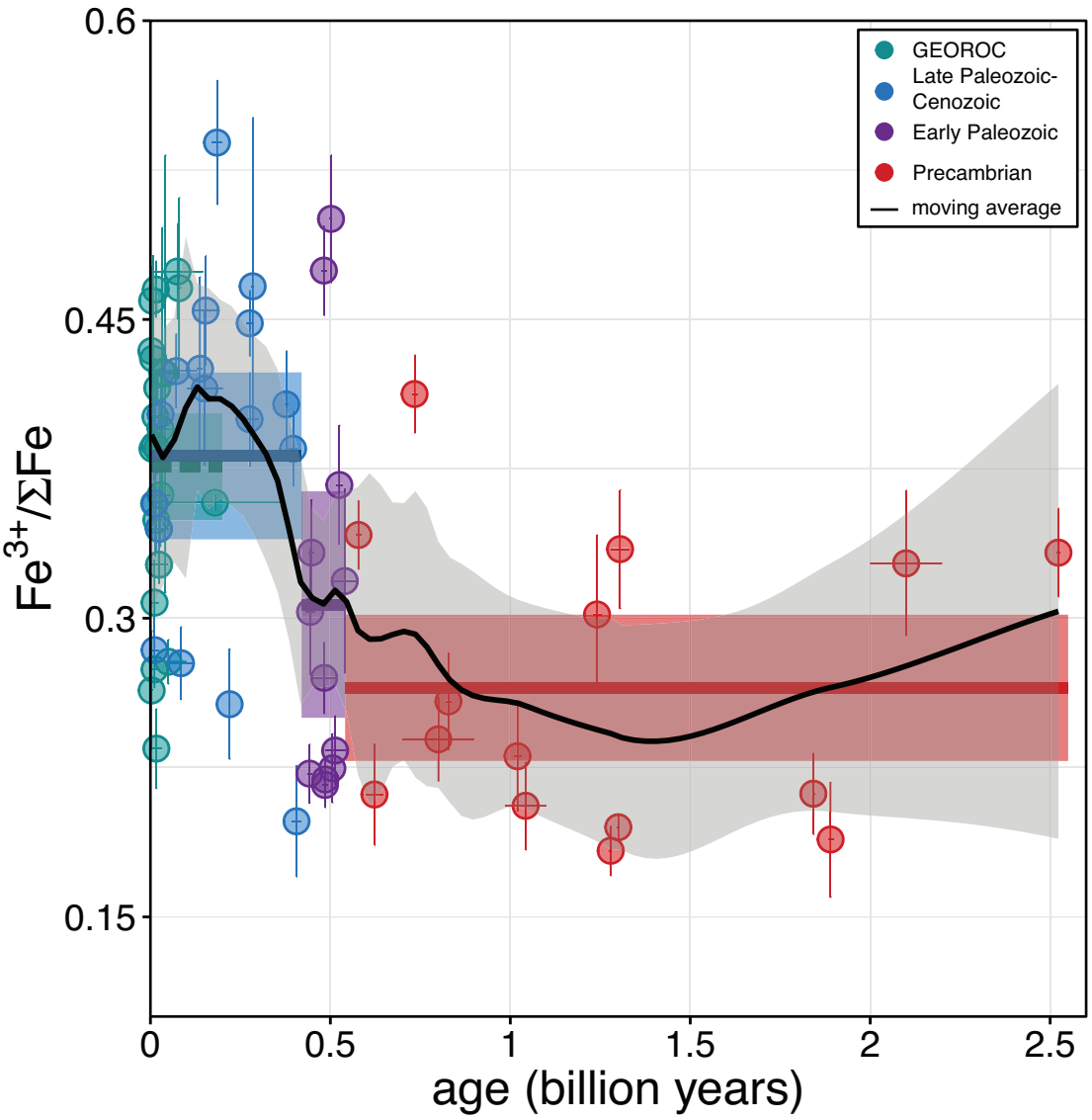

Fig. S2. $Fe^{3+}/\Sigma Fe$ ratios vs. age with a moving average. The $Fe^{3+}/\Sigma Fe$ ratios (as given in Fig. 1) are presented here along with a moving average (black line) through the data with 95% confidence interval (gray outline). The moving average indicates an increase in $Fe^{3+}/\Sigma Fe$ ratios after the Neoproterozoic and sometime between the Early and Late Paleozoic. This provides independent support for our choice of age bins to compare the mean $Fe^{3+}/\Sigma Fe$ ratios of Precambrian vs. Late Paleozoic localities. The moving average was calculated using the R software package with the built-in 'loess' method using a span of 0.25 (which can range from 0-1 and represents the smoothing window size). Choice of a different span (0.1-0.5) does not change our conclusions.

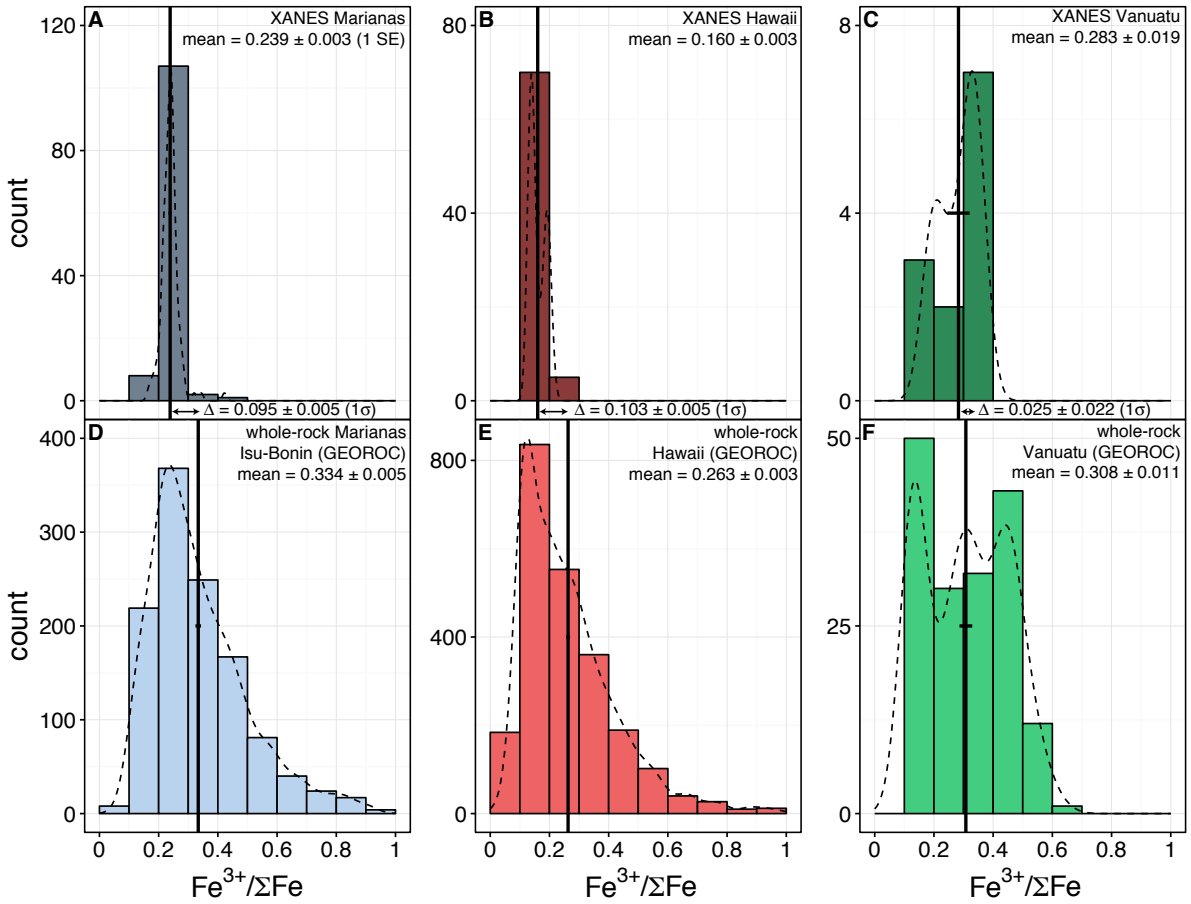

Fig. S3. Comparison $Fe^{3+}/\Sigma Fe$ ratios measured by XANES (A, B, and C) and whole-rock measurements from the GEOROC database (D, E, F). Solid black vertical lines are the mean, with horizontal 2 SE error bars. Mean values for each distribution are given in the upper right of each plot along with the one standard error. Dotted lines are smoothed distributions. Differences between XANES and whole-rock data are given by the Δ between the histograms along with 1σ errors based on the propagation of error. $Fe^{3+}/\Sigma Fe$ ratios for whole-rock analyses are elevated by 0.074 on average compared to XANES measurements from the same locality. XANES data for the Marianas are from (7, 10, 11). XANES data for Vanuatu are from (12). For Hawaii, XANES data are from (13). Whole-rock data are from GEOROC for all localities examined.

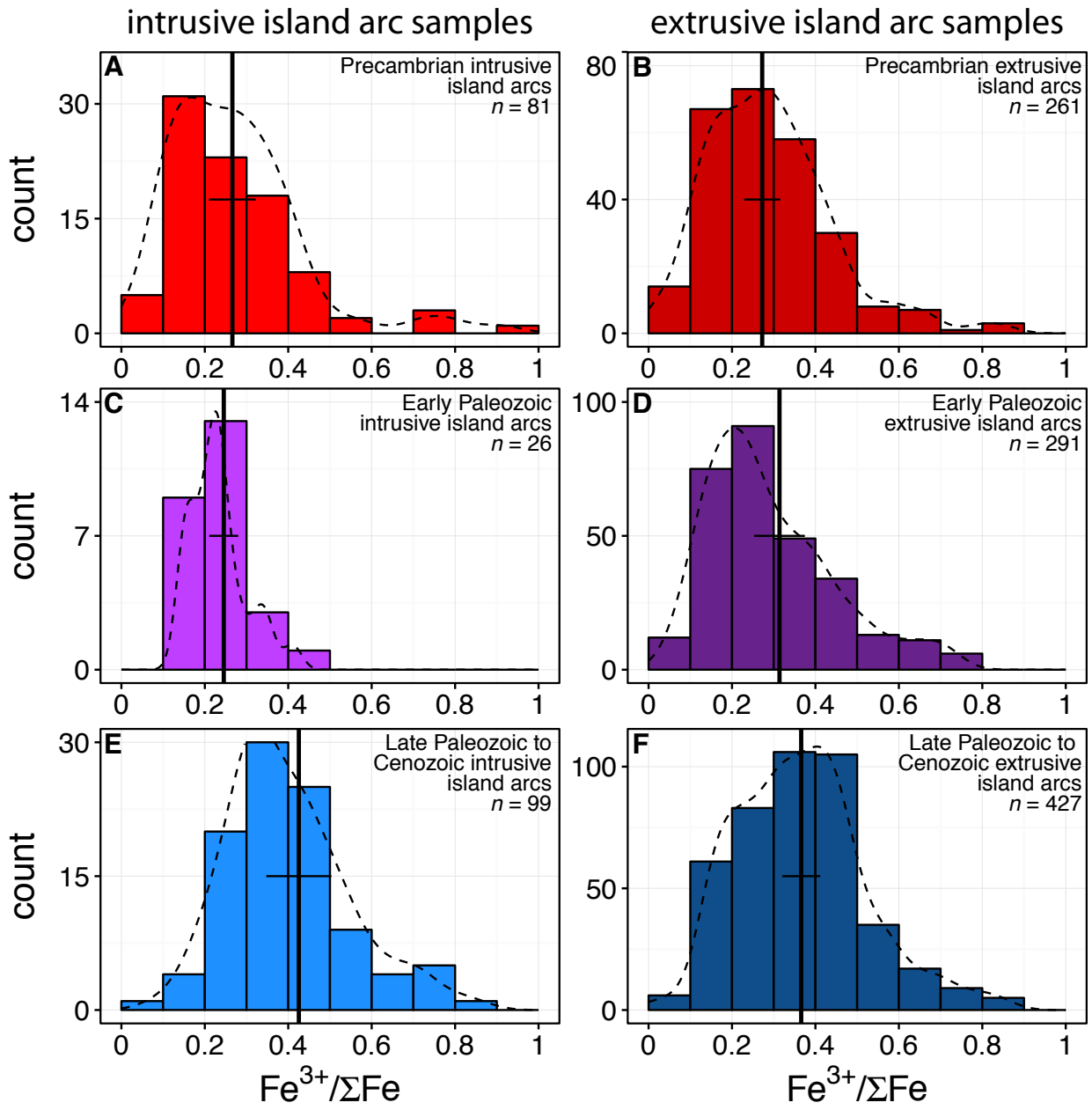

Fig. S4. Histograms of $Fe^{3+}/\Sigma Fe$ data for intrusive (A, B, E) vs. extrusive (B, D, F) island arc rocks. Black vertical lines are the average value of the formational averages for a given time bin with 2 SE error bars. *n* is the number of data points. All data are included, even if a locality only has one data point, and thus *n* here can be larger than *n* in Table S2. Dotted lines are smoothed distributions.

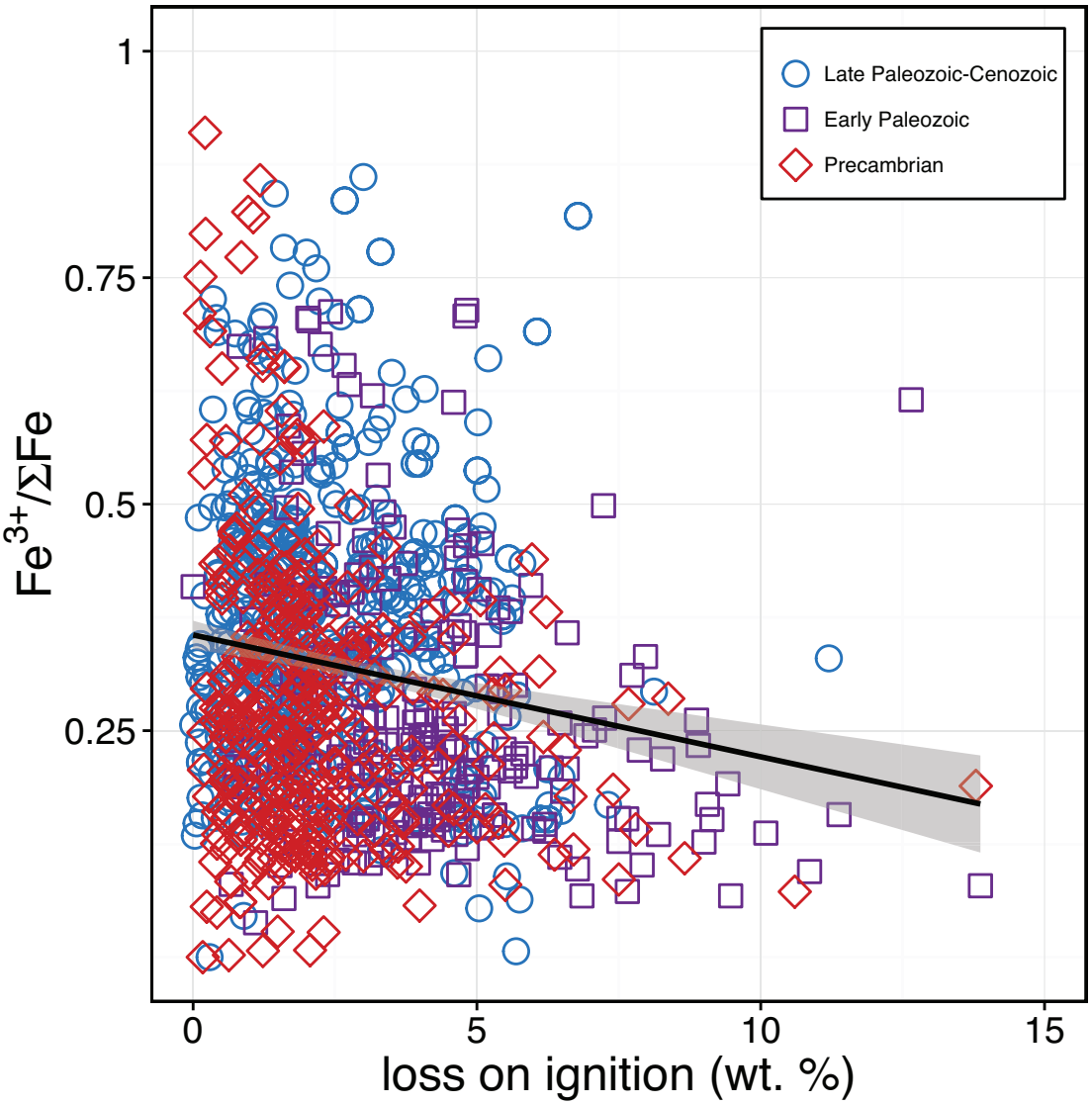

Fig. S5. $Fe^{3+}/\Sigma Fe$ ratios vs. loss on ignition (LOI) of compiled samples. The dependence of $Fe^{3+}/\Sigma Fe$ vs. LOI (see black line with 95% confidence interval above) is weak with a slope of -0.0135 (±0.002, 1 SE) and with a R^2 value of 0.027. Given that the average LOI of the Precambrian (2.12 ± 0.09, 1 SE) and Late Paleozoic-Cenozoic (2.39 ± 0.07) samples overlap at the 2 SE level, the observed weak dependence between LOI and $Fe^{3+}/\Sigma Fe$ cannot explain the observed mean difference of ~0.1 in $Fe^{3+}/\Sigma Fe$ between Precambrian and Late Paleozoic-Cenozoic samples.

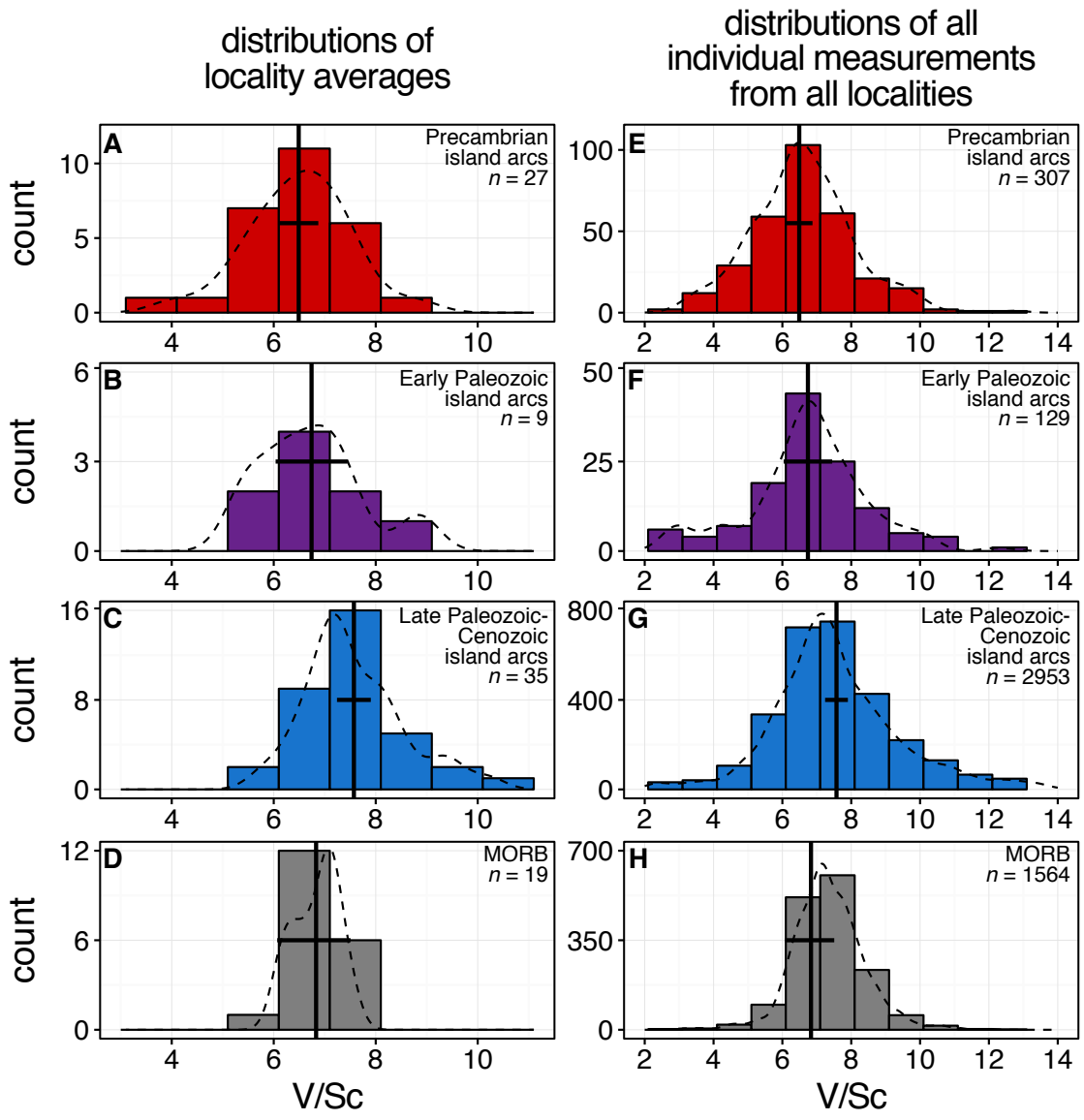

Fig. S6. Histograms of V/Sc data. A-D are histograms of the locality averages (as given in Fig. 2). E-H are histograms of every individual data point used to calculate the locality averages**.** Black vertical lines are the average value of the locality averages for a given time bin with 2 SE error bars as given in Fig. 2. *n* is the number of data points. Dotted lines are smoothed distributions. The Late Paleozoic-Cenozoic age range includes data compiled by us and from GEOROC. All island arc data (A-C and E-G) have been filtered for MgO content such that samples have between 6.5-15 wt. % MgO. MORB data is from (14) with data filtered for MgO contents between 8-15 wt. % MgO. For the individual data points, for visual clarity, we have restricted the V/Sc ratio range to between 2 and 14. There are a small number of points outside of this range including one point from the Precambrian dataset with a value of 15.1; two points from the Early Paleozoic dataset between 14.3 and 16.4; and 12 points from 0.05-2, 35 points from 14.0-32.3, and one elevated point at 57.5 from the Late Paleozoic-Cenozoic dataset (See Dataset S3). A shift in the mean and mode of the distributions to higher V/Sc ratios for the Late Paleozoic-Cenozoic samples relative to early time frames (Early Paleozoic and Precambrian) is apparent for the locality averages (A-D). This shift is also present when looking at all of the distributions of the individual data points (E-H), but is clearly less visually obvious given the large absolute range of V/Sc ratios.

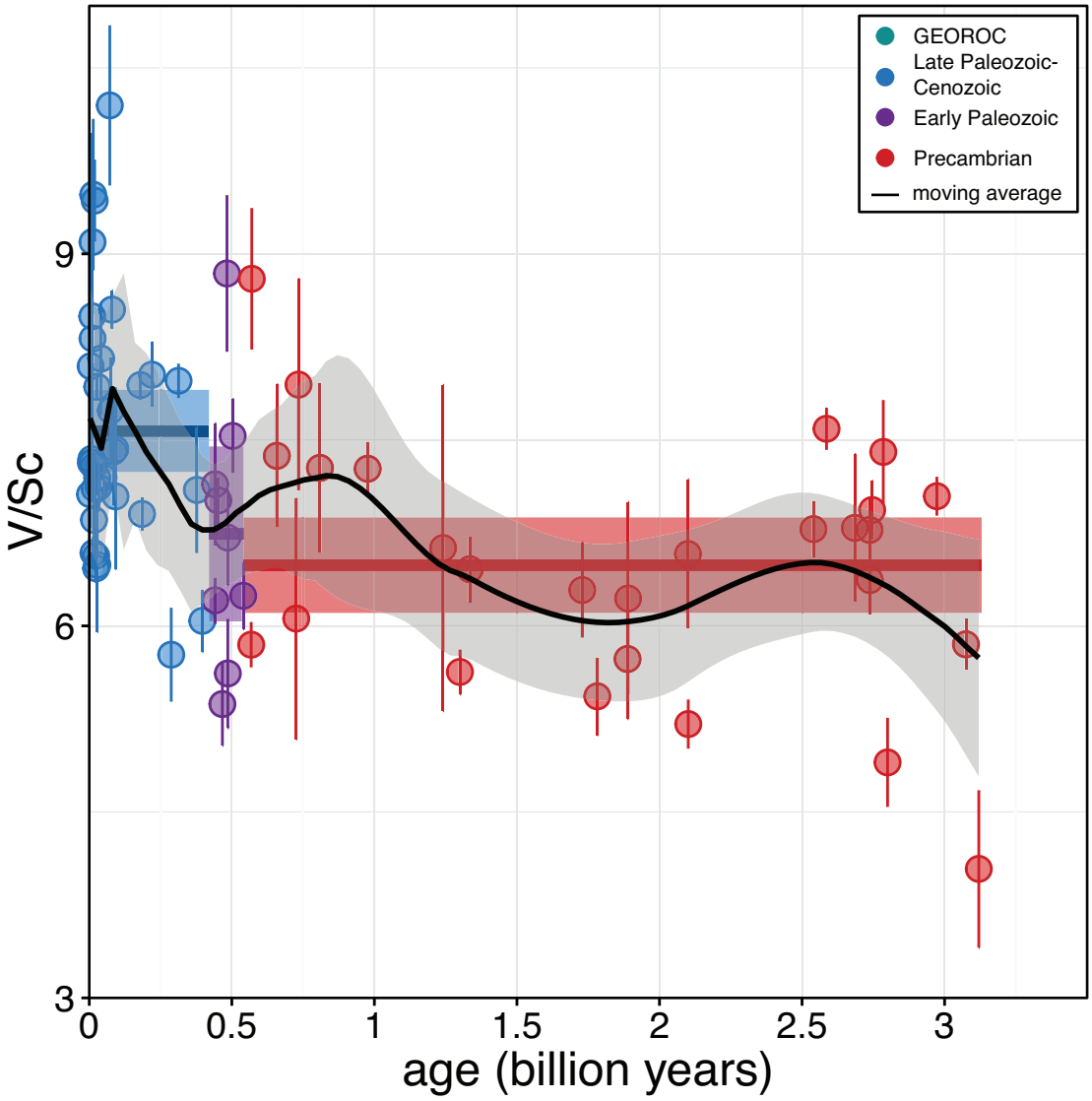

Fig. S7. V/Sc ratios vs. age with a moving average. The V/Sc ratios (as given in Fig. 1) are presented here along with a moving average (black line) through the data with 95% confidence interval (gray outline). The moving average shows an increase in V/Sc after the Neoproterozoic and sometime between the Early and Late Paleozoic. This provides independent support for our choice of age bins in order to compare mean $Fe^{3+}/\Sigma Fe$ and V/Sc ratios Precambrian vs. Late Paleozoic localities. The moving average was calculated with the R software package using the built-in 'loess' method with a span of 0.25 (which can range from 0-1 and represents the smoothing window size). Choice of a different span (0.2-0.5) does not change our conclusions.

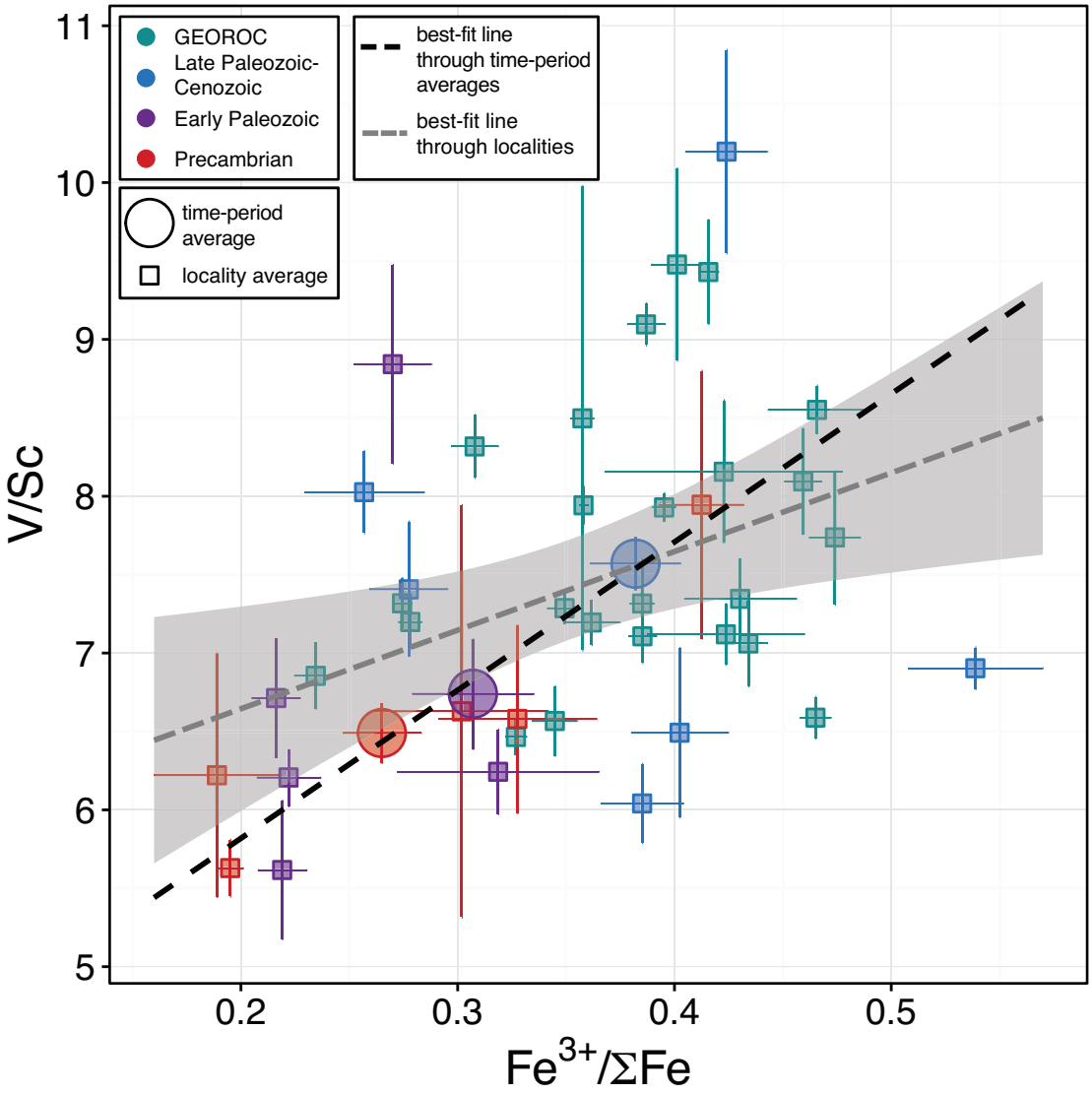

Fig. S8. V/Sc vs. $Fe^{3+}/\Sigma Fe$ ratios. Large circles are time-period averages with a dotted-black-line linear regression fit to the data. In smaller squares are locality averages with both V/Sc and $Fe^{3+}/\Sigma Fe$ ratios with a dotted-grey-line linear regression fit to the data and a grey 95% confidence interval. Note these ratios are generally not measured on the same rocks, and sometimes are not from the same study. Only 1/3 of localities examined (other than the GEOROC database) had both V/Sc and $Fe^{3+}/\Sigma Fe$ ratios making full comparison difficult. For example, only 5 Precambrian localities had both ratios measured. Despite this, and the clear scatter, the locality averages still show a positive slope as would be expected based on the time-period averages.

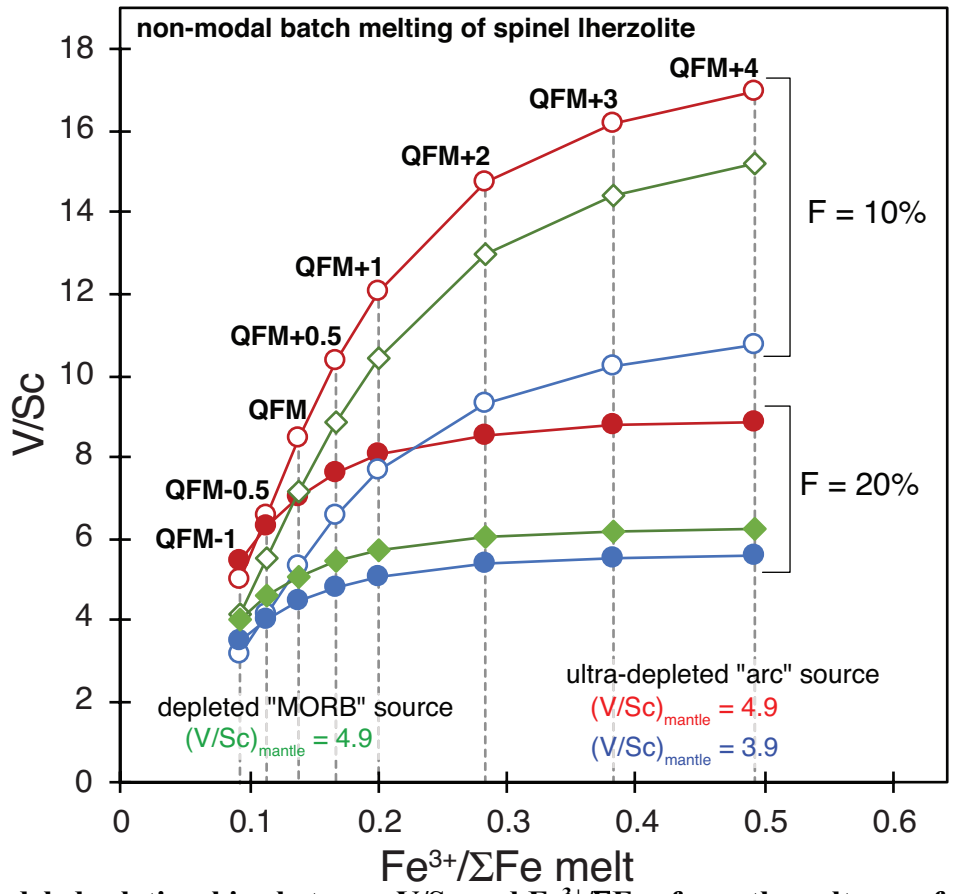

Fig. S9. Modeled relationships between V/Sc and $Fe^{3+}/\Sigma Fe$ of mantle melts as a function of the fO_2 of the source, degree of melting (F), and initial V/Sc ratio. The results are derived from a non-modal batch melting model of a spinel lherzolite source. The details of the model are given in the Supplementary Information Text (above). The model was run to capture fO_2 values from 1 log unit below to 4 log units above the quartz-fayalite-magnetite (QFM) buffer. These ranges bracket the typical estimated ranges for the fO_2 of both MORB and island arc rocks (e.g., refs. 7, 15–17). Model results are given for melting fractions (F) of 10% and 20%, which are the typical range for island arcs. We examine scenarios in which there has not been prior mantle melting of the source of island arcs (green curve) as well as scenarios in which that has been some melt extraction (e.g., at a back arc spreading center; red and blue curves). Prior melt extraction is simulated through a change in source mineralogy (red and blue curves) combined with a decrease in source V/Sc ratio (blue curve only), which both change V/Sc as a function of the fO_2 (4). Vertical grey dotted lines provide guidance for the $Fe^{3+}/\Sigma Fe$ ratio of the rock at a given fO_2 of the melt relative to the QFM buffer.

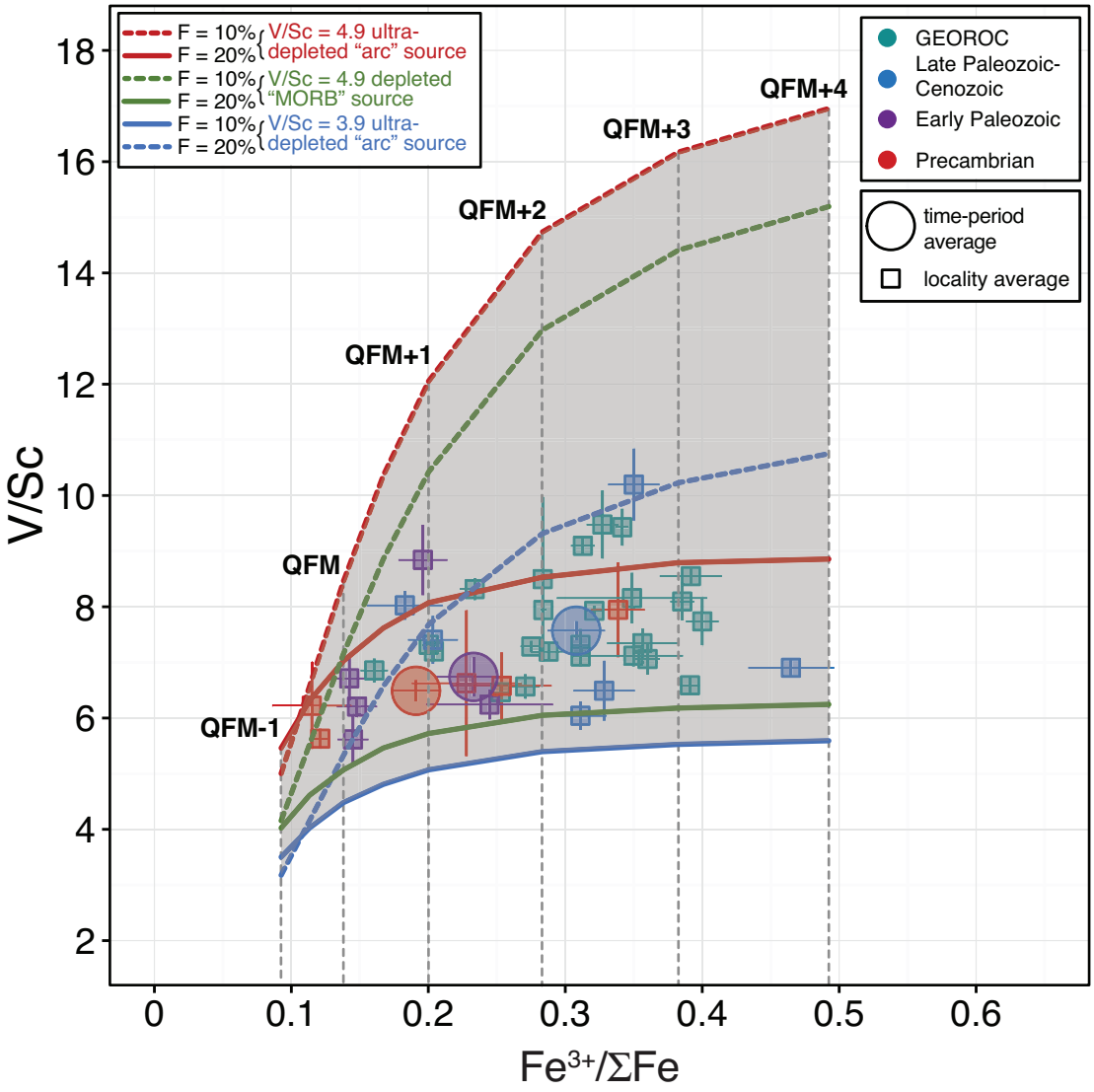

Fig. S10. Comparison of the $Fe^{3+}/\Sigma Fe$ (corrected for post formational oxidation) and V/Sc ratios of localities as given in Fig. S8 vs. the model results given in Fig. S9. See Fig. S8 and Fig. S9 for details on the data and the model. We have subtracted 0.074 from all $Fe^{3+}/\Sigma Fe$ ratios in order to correct for secondary oxidation of the samples inferred based on the observed difference between whole-rock and XANES measurements (see main text and Fig. S3). Phanerozoic $Fe^{3+}/\Sigma Fe$ ratios fall between estimated fO_2 values relative to the quartz-fayalite-magnetite (QFM) buffer of 0 to +4 log units, within the typical range estimated for island arc rocks (e.g., refs. 7, 15–17). The data fall within the range of plausible space defined by the model (as given in the grey shaded area). They appear to generally fall within the space outlined by a high degree melts (20% melting) for either a MORB like source or a source with prior melt extraction with initial V/Sc ratios of 4.9 in both cases. The key point is that the data fall within the space given by our model and expected ranges of fO_2 values for island arc rocks based on prior results.

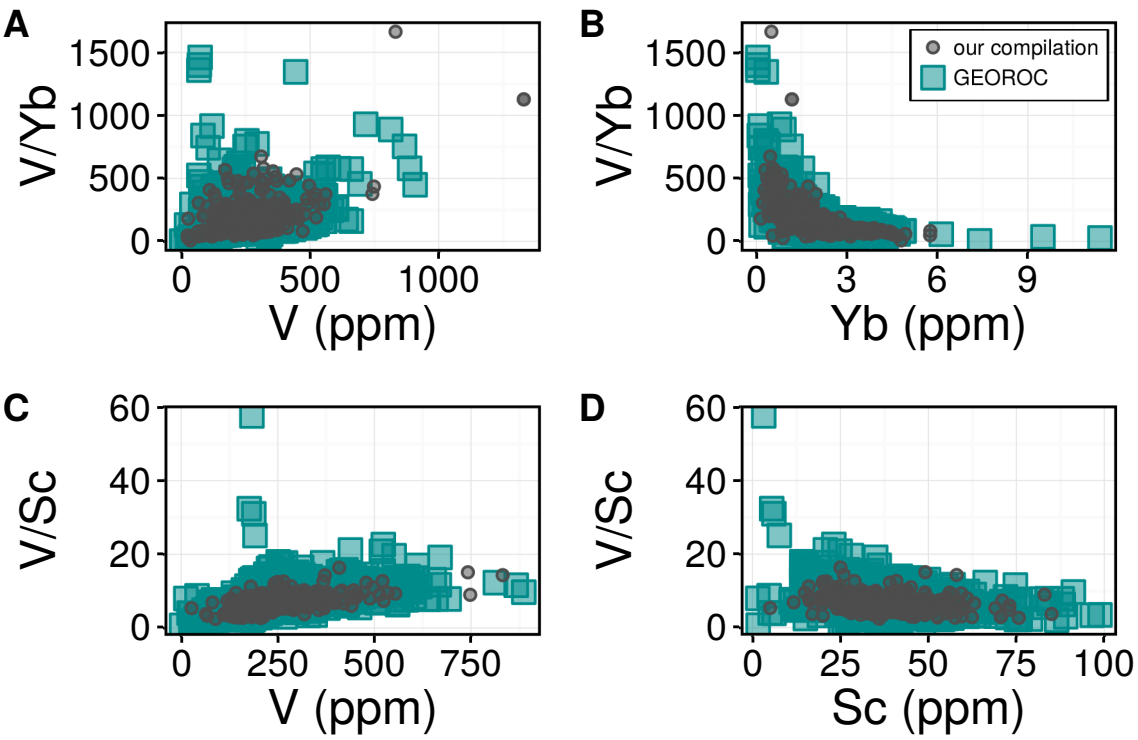

Fig. S11. Comparison of V/Yb and V/Sc ratios to whole-rock V, Yb, and Sc concentrations for samples complied here (black circles) and the GEOROC database (cyan squares). Samples have been filtered such that MgO contents are between 6.5-15 wt. %. V/Yb ratios show a hyperbolic relationship vs. Yb content (B), with strong curvature apparent below ~2 ppm Yb. We interpret this curvature to result, in part, from imprecise measurements at low Yb concentrations, which due to the already low Yb contents of arc rocks, drives V/Yb ratios to artificially high values. 61% of the GEOROC samples and 62% of samples we compiled have Yb contents less than 2 ppm, making use of V/Yb ratios in our dataset as a quantitative oxybarometer problematic, and, as a result, we do not use it here. In contrast, V/Sc ratios do not show an obvious hyperbolic relationship with respect to Sc. Although there is an increase in V/Sc ratios at low Sc (<15 ppm) in the GEOROC dataset, only 4 samples are clearly elevated (C and D). Removal of these four samples changes the mean V/Sc ratio of the Late Paleozoic-Cenozoic time period from 7.56 ± 0.16 (1 SE) to 7.53 ± 0.15. Thus, we consider V/Sc ratios, in part due to higher Sc contents of most arc rocks (>20 ppm typically) to be less susceptible to measurement imprecision on the denominator.

Table S1 $Fe^{3+}/\Sigma Fe$ of island arc rocks vs. SiO_2, MgO, and FeO wt. % for various age bins. Values are means of locality averages for a given age range. Some data do not include major element information, and we filter those data out for the "all with majors" filter category. For the filtered data, only locations with at least two samples were used post filtering. $\Delta_{all\text{-}filter}$ is the difference between the value for whatever filter is applied vs. when all data is averaged for a given time period. For SiO_2 and MgO this difference is taken only to data with major element data ('all with majors'). For the $Fe^{3+}/\Sigma Fe$ data, the difference is to all data ('all').

	<420 Ma				420-541 Ma				>541 Ma			
filter	mean	1 SE	$\Delta_{all\text{-}filter}$	% remaining	mean	1 SE	$\Delta_{all\text{-}filter}$	% remaining	mean	1 SE	$\Delta_{all\text{-}filter}$	% remaining
all	0.382	0.021	0.000	100	0.307	0.028	0.015	100	0.265	0.018	0.000	100
all with majors	0.382	0.021	0.000	100	0.292	0.026	0.000	93	0.265	0.018	0.000	100
<70% SiO_2	0.377	0.021	-0.005	97	0.285	0.026	-0.006	88	0.260	0.017	-0.005	91
<65% SiO_2	0.369	0.021	-0.013	91	0.278	0.023	-0.014	84	0.253	0.016	-0.012	83
<60% SiO_2	0.365	0.022	-0.016	84	0.272	0.021	-0.020	77	0.254	0.015	-0.011	74
>1% MgO	0.377	0.021	-0.005	97	0.286	0.026	-0.006	87	0.259	0.017	-0.006	90
>2% MgO	0.370	0.021	-0.012	89	0.274	0.023	-0.018	81	0.255	0.016	-0.010	82
>3% MgO	0.365	0.022	-0.016	79	0.265	0.018	-0.027	72	0.254	0.016	-0.011	78
>4% MgO	0.362	0.025	-0.019	64	0.266	0.019	-0.025	64	0.254	0.015	-0.011	68
>5% MgO	0.346	0.032	-0.036	48	0.249	0.022	-0.042	52	0.248	0.015	-0.017	59
>6% MgO	0.334	0.038	-0.047	38	0.231	0.024	-0.061	40	0.246	0.014	-0.019	45
<80% $Fe^{3+}/\Sigma Fe$	0.378	0.021	-0.004	99	0.307	0.028	0.000	100	0.263	0.017	-0.002	99
<70% $Fe^{3+}/\Sigma Fe$	0.371	0.020	-0.011	96	0.299	0.027	-0.008	98	0.260	0.017	-0.005	98
<60% $Fe^{3+}/\Sigma Fe$	0.356	0.018	-0.026	92	0.287	0.024	-0.020	95	0.256	0.016	-0.009	96
<50% $Fe^{3+}/\Sigma Fe$	0.338	0.016	-0.043	84	0.279	0.021	-0.028	91	0.250	0.015	-0.015	93

Table S2. $Fe^{3+}/\Sigma Fe$ of island arc rocks as a function of emplacement style. Values are the mean of locality averages for a given age range. Only localities with two or more samples were included and where sample emplacement style is known. Data for 'all' includes samples with unknown emplacement style (hence why the number of samples for the 'volcanic' and 'intrusive' categories do not necessarily equal the number of samples for the 'all' category).

	<420 Ma			420-541 Ma			>541 Ma		
dataset	mean $Fe^{3+}/\Sigma Fe$	1 SE	*n*	mean $Fe^{3+}/\Sigma Fe$	1 SE	*n*	mean $Fe^{3+}/\Sigma Fe$	1 SE	*n*
all	0.382	0.021	528	0.307	0.028	317	0.265	0.018	367
volcanic	0.366	0.023	427	0.314	0.030	291	0.272	0.022	261
intrusive	0.425	0.039	97	0.245	0.017	25	0.266	0.028	81

Additional Datasets

Dataset S1: Locality descriptions (available on line)

Dataset S2: $Fe^{3+}/\Sigma Fe$ ratios of island arc rocks through time (available on line)

Dataset S3: Mean $Fe^{3+}/\Sigma Fe$ ratios of island arc localities through time (available on line)

Dataset S4: V/Sc ratios of island arc rocks through time (available on line)

Dataset S5: Mean V/Sc ratios of island arc localities through time (available on line)

References

1. Schmidt MW, Jagoutz O (2017) The global systematics of primitive arc melts. *Geochem Geophys Geosyst* 18(8):2817–2854.

2. Shaw DM (1970) Trace element fractionation during anatexis. *Geochim Cosmochim Acta* 34(2):237–243.

3. Kinzler RJ (1997) Melting of mantle peridotite at pressures approaching the spinel to garnet transition: Application to mid-ocean ridge basalt petrogenesis. *JGR Solid Earth* 102(B1):853–874.

4. Prytulak J, et al. (2016) Stable vanadium isotopes as a redox proxy in magmatic systems? *Geochem Perspect Lett* 3(1):75–84.

5. Salters VJ, Stracke A (2004) Composition of the depleted mantle. *Geochem Geophys Geosyst* 5(5).

6. Mallmann G, O'Neill HSC (2009) The crystal/melt partitioning of V during mantle melting as a function of oxygen fugacity compared with some other elements (Al, P, Ca, Sc, Ti, Cr, Fe, Ga, Y, Zr and Nb). *J Petrol* 50(9):1765–1794.

7. Brounce M, Kelley K, Cottrell E (2014) Variations in $Fe^{3+}/\Sigma Fe$ of Mariana arc basalts and mantle wedge fO_2. *J Petrol* 55(12):2513–2536.

8. Kress VC, Carmichael IS (1991) The compressibility of silicate liquids containing Fe_2O_3 and the effect of composition, temperature, oxygen fugacity and pressure on their redox states. *Contrib Mineral Petrol* 108(1–2):82–92.

9. Frost BR (1991) Introduction to oxygen fugacity and its petrologic importance. *Rev Mineral Geochem* 25(1):1–9.

10. Kelley KA, Cottrell E (2012) The influence of magmatic differentiation on the oxidation state of Fe in a basaltic arc magma. *Earth Planet Sci Lett* 329:109–121.

11. Brounce M, Kelley KA, Cottrell E, Reagan MK (2015) Temporal evolution of mantle wedge oxygen fugacity during subduction initiation. *Geology* 43(9):775–778.

12. Gentes Z (2015) Near-Primary Mantle Melts and Their Implications for the Mechanism of Island Arc Basalt Oxidation. Master's thesis (University of Rhode Island, Kingston, RI).

13. Brounce M, Stolper E, Eiler J (2017) Redox variations in Mauna Kea lavas, the oxygen fugacity of the Hawaiian plume, and the role of volcanic gases in Earth's oxygenation. *Proc Natl Acad Sci* 114(34):8997–9002.

14. Gale A, Dalton CA, Langmuir CH, Su Y, Schilling J (2013) The mean composition of ocean ridge basalts. *Geochem Geophys Geosyst* 14(3):489–518.

15. Ballhaus C, Berry RF, Green DH (1990) Oxygen fugacity controls in the Earth's upper mantle. *Nature* 348(6300):437.

16. Carmichael IS (1991) The redox states of basic and silicic magmas: a reflection of their source regions? *Contrib Mineral Petrol* 106(2):129–141.

17. Evans K, Elburg M, Kamenetsky V (2012) Oxidation state of subarc mantle. *Geology* 40(9):783–786.